Regulated Fast Nucleocytoplasmic Shuttling Observed by Reversible Protein Highlighting

Ryoko Ando, *et al.*

Science **306**, 1370 (2004);
DOI: 10.1126/science.1102506

0.005 to 0.04 per billion years, respectively) are similar to the estimate from genes with $T_m = T_0$, which is not expected if the gene loss rate is much higher than the gene duplication rate.

The data also allow us to quantify the duration of concerted evolution and the level of gene conversion. The question of the duration of concerted evolution is addressed according to the recent theoretical result of Teshima and Innan (*8*), who showed that the period of concerted evolution approximately follows an exponential distribution with parameter $1/\tau$, where τ is the expected length of concerted evolution. The probability (f) that the duration of concerted evolution from a certain time point (t_s) exceeds another time point (t_e) is given by $\exp[-(t_e - t_s)/\tau]$. To estimate τ assuming a constant τ for all gene pairs, we considered two time points, T_4 and T_1, on the species tree (Fig. 1A). We focused on the 51 gene pairs for which concerted evolution was likely occurring at T_4. For each of these 51 gene pairs, we considered whether concerted evolution was still going on at T_1 by comparing *Ks* among four gene sequences, two from *S. cerevisiae* and two from *S. paradoxus*. We found smaller values of *Ks* between the paralogs within species than between orthologs for nine gene pairs that were considered to be under concerted evolution at T_1. We could then estimate $f = 9/51$, from which an estimate of $\tau = 0.2$ was obtained by solving $\exp(-0.35/\tau) = f$, where 0.35 is the time between T_1 and T_4 measured in units of $1/Ks$. Assuming the synonymous substitution rate $Ks = 8.1 \times 10^{-9}$, the estimate yields $\tau = 25$ million years (*13*).

The rate of gene conversion is one of the important factors in determining the period of concerted evolution. The gene conversion rate can be directly estimated from the nucleotide divergence between gene pairs currently under concerted evolution. Because it was not possible to determine such gene pairs, we used the nine gene pairs that are likely under concerted evolution at T_1 as a proxy, for which the average $d = 0.036$. The expectation of d is given by μ/c, where μ is the mutation rate per site and c is the gene conversion rate per site (*17*, *18*); hence, we estimate that the gene conversion rate is ~28 times the mutation rate, assuming that c is constant for all duplicated genes (*13*). This is within the range of estimates (10 to 100) in *Drosophila* duplicated genes (*18*).

Our demonstration of extensive concerted evolution via gene conversion on a genome scale is consistent with molecular genetic studies showing frequent interlocus gene conversion in yeast (*19*). Although yeast is a model species for studying gene conversion, there is no reason to believe that the effect of gene conversion in duplicated genes is negligible in other organisms. Increasing evidence for gene conversion (interlocus as well as intralocus) is also available in higher eukaryotes, such as humans (*20–23*), *Drosophila* (*18*, *24*, *25*), and other species (*26*).

References and Notes

1. S. Ohno, *Evolution by Gene Duplication* (Springer-Verlag, New York, 1970).
2. W.-H. Li, *Molecular Evolution* (Sinauer, Sunderland, MA, 1997).
3. M. Lynch, J. S. Conery, *Science* **290**, 1151 (2000).
4. E. Zuckerkandl, L. Pauling, in *Evolving Genes and Proteins*, V. Bryson, H. J. Vogel, Eds. (Academic Press, New York, 1965), pp. 97–166.
5. T. Ohta, *Evolution and Variation of Multigene Families* (Springer-Verlag, Berlin, 1980).
6. G. Dover, *Nature* **299**, 111 (1982).
7. J. F. Elder Jr., B. J. Turner, *Q. Rev. Biol.* **70**, 297 (1995).
8. K. M. Teshima, H. Innan, *Genetics* **166**, 1553 (2004).
9. A. Gofieau *et al.*, *Science* **274**, 546 (1996).
10. P. Cliften *et al.*, *Science* **301**, 71 (2003).
11. M. Kellis, N. Patterson, M. Endrizzi, B. Birren, E. S. Lander, *Nature* **423**, 241 (2003).
12. A. Rokas, B. L. Williams, N. King, S. B. Carroll, *Nature* **425**, 798 (2003).
13. See supporting data on *Science* Online.
14. B. Walsh, *Genetica* **118**, 279 (2003).
15. K. Wolfe, D. Shields, *Nature* **387**, 708 (1997).
16. M. Kellis, B. W. Birren, E. S. Lander, *Nature* **428**, 617 (2004).
17. T. Ohta, *Proc. Natl. Acad. Sci. U.S.A.* **79**, 3251 (1982).
18. H. Innan, *Genetics* **163**, 803 (2003).
19. T. D. Petes, C. W. Hill, *Annu. Rev. Genet.* **22**, 147 (1988).
20. S. Rozen *et al.*, *Nature* **423**, 873 (2003).
21. H. Innan, *Proc. Natl. Acad. Sci. U.S.A.* **100**, 8793 (2003).
22. M. E. Hurles, D. Willey, L. Matthews, S. S. Hussain, *Genome Biol.* **5** (8), 10.1186/gb-2004-5-8-r55 (2004).
23. A. J. Jeffreys, C. A. May, *Nature Genet.* **36**, 151 (2004).
24. C. H. Langley, B. P. Lazzaro, W. Phillips, E. Heikkinen, J. M. Braverman, *Genetics* **156**, 1837 (2000).
25. W. Wang, K. Thornton, J. J. Emerson, M. Long, *Genetics* **166**, 1783 (2004).
26. G. Marais, *Trends Genet.* **19**, 330 (2003).
27. Z. Yang, R. Nielsen, *Mol. Biol. Evol.* **17**, 32 (2000).

28. We thank S. A. Barton, Y.-X. Fu, Z. Gu, Y. Jin, M. Long, M. Nordborg, T. Ohta, N. Rosenberg, K. M. Teshima, K. Thornton, three anonymous referees for comments, and A. Rokas for data. H.I. is supported by a grant from the University of Texas.

Supporting Online Material

www.sciencemag.org/cgi/content/full/306/5700/1367/DC1
Materials and Methods
SOM Text
Table S1
Figs. S1 and S2
References

28 June 2004; accepted 4 October 2004

Regulated Fast Nucleocytoplasmic Shuttling Observed by Reversible Protein Highlighting

Ryoko Ando, Hideaki Mizuno, Atsushi Miyawaki*

The observation of the regulation of fast protein dynamics in a cellular context requires the development of reliable technologies. Here, a signal regulation cascade reliant on the stimulus-dependent acceleration of the bidirectional flow of mitogen-activated protein kinase (extracellular signal-regulated kinase) across the nuclear envelope was visualized by reversible protein highlighting. Light-induced conversion between the bright and dark states of a monomeric fluorescent protein engineered from a novel coral protein was employed. Because of its photochromic properties, the protein could be highlighted, erased, and highlighted again in a nondestructive manner, allowing direct observation of regulated fast nucleocytoplasmic shuttling of key signaling molecules.

Fluorescent proteins isolated from cnidaria have been used to generate fusion tags that act as fluorescent reporters for studying protein dynamics (*1–3*). However, tracking protein behavior is difficult when the tagged protein is evenly distributed under steady-state conditions. Fluorescence recovery after photobleaching (FRAP) and optical highlighting of fluorescent proteins can provide insights into the diffusive or directed movement of proteins and track rapid protein behavior (*4–7*), but protein movement is regulated by many different factors and may be altered by changes in the cellular state. Because photobleaching, photoactivation, and photoconversion with the available markers are often irreversible or complex, the identification of genetically encoded fluorescent proteins that can be marked reversibly for repeated measurements of protein behavior has long been pursued.

We prepared a cDNA library from Pectiniidae, a species of coral that emits faint fluorescence upon irradiation with ultraviolet light. Approximately 300,000 bacterial colonies containing individual cDNA clones were screened for fluorescence (*8*). A single clone (22G) encoding a greenish fluorescent protein with highest homology to mcavGFP

Laboratory for Cell Function and Dynamics, Advanced Technology Development Group, Brain Science Institute, RIKEN, 2-1 Hirosawa, Wako-city, Saitama, 351-0198, Japan.

*To whom correspondence should be addressed. E-mail: matsushi@brain.riken.jp

(*9*) (74.6%) was identified. Recombinant 22G protein was expressed in *E. coli* and purified, and its molecular mass determined to be 102 kD by analytical equilibrium ultracentrifugation analysis. This was 3.5 times as large as that predicted from the primary structure of the protein (29.2 kD), which suggests that 22G forms an oligomeric complex (*2*). We engineered a monomeric version of 22G (22Gm3) by introducing both rational and random mutations (*10*) (fig. S1). The molecular mass of 22Gm3 was measured to be 28.8 kD.

The absorption spectrum of 22Gm3 at pH 7.4 displayed a major peak at 503 nm (ε = 95,000 $M^{-1}\cdot cm^{-1}$) and a minor peak at 390 nm. The amplitude of the 503-nm peak decreased with decreasing pH, whereas that of the 390-nm peak increased, exhibiting an isosbestic point at 428 nm (Fig. 1A). The 390- and 503-nm peaks correspond respectively to the neutral and ionized states of the phenolic hydroxyl of the chromophore (*1*). The apparent pK_a was 5. Excitation and emission spectra of 22Gm3 were analyzed (Fig. 1C). The neutral form was nonfluorescent, but the ionized form was highly fluorescent, with an emission maximum of 518 nm. The fluorescence quantum yield (Φ_{FL}) was 0.85.

We found 22Gm3 to possess a distinctive photosensitivity. Strong excitation at around 490 nm appeared to bleach 22Gm3 more efficiently than other fluorescent proteins, and the bleached protein regained its green fluorescence completely with minimal irradiation at around 400 nm. We intermittently measured the absorbance of a solution containing 22Gm3 at pH 7.4 in a cuvette during continuous illumination at 490 ± 10 nm with a 75-W xenon lamp (Fig. 1B). After a 40-min incubation, nearly all the protein molecules had been converted into the neutral, nonfluorescent state. Illumination at 400 ± 7.5 nm for several minutes reversed the protein to its original fluorescent state (Fig. 1B). Thus, 22Gm3 has photochromic behavior, because its fluorescence can be switched on and off by using two different wavelengths of light. This photochromism is not pH sensitive, because the neutral state generated by acidification was unaffected by illumination with 400-nm light (fig. S2). Based on the capacity of its fluorescence to vanish and reappear, 22Gm3 was renamed "Dronpa," after "dron," a ninja term for vanishing, and "pa," which stands for photoactivation.

The kinetics of the photochromic behavior of Dronpa were explored in cells by microscopy (*8*). When Dronpa was transfected into HeLa cells, green fluorescence was uniformly distributed in both cytosolic and nuclear compartments (Fig. 1D). Fluorescence was monitored in fixed cell samples subjected to strong irradiation at 400 or 490 nm (Fig. 1E). Photoactivation of Dronpa required much less photon energy than did

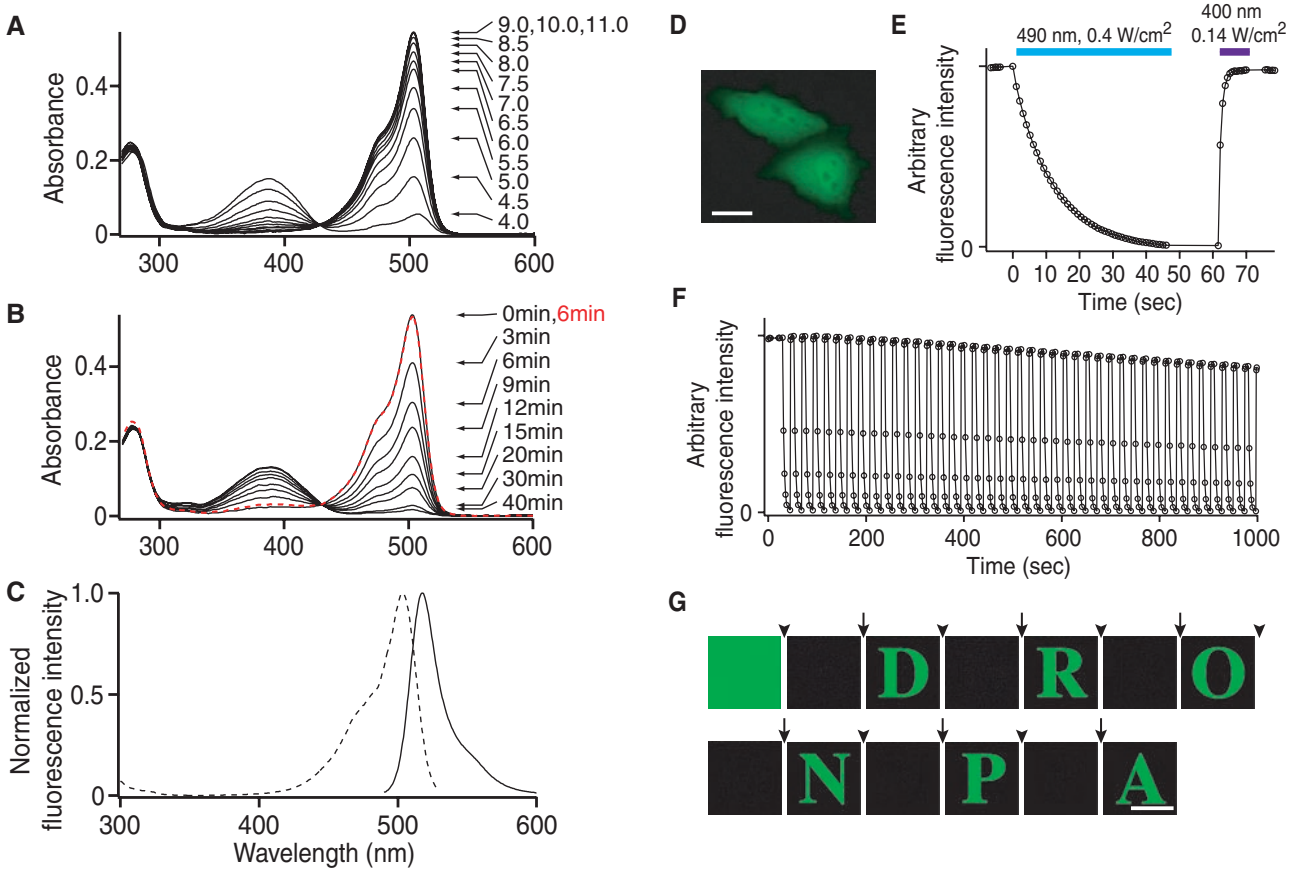

Fig. 1. Photochromic properties of Dronpa (22Gm3). (**A**) The pH dependence of 22Gm3 absorbance. (**B**) Irradiation-dependent changes in 22Gm3 absorbance. Absorbance spectra obtained during irradiation at 490 nm (black) and after irradiation at 400 nm (red) are displayed. (**C**) Normalized excitation (dotted line) and emission (solid line) spectra of 22Gm3. (**D**) Fluorescence micrograph of HeLa cells expressing Dronpa. Scale bar, 20 μm. (**E**) Time course of intensity of Dronpa fluorescence in a fixed HeLa cell. Green fluorescence was monitored by using a 490DF20 excitation filter overlaid with a 0.3% transmittance neutral density (ND) filter, a 505DRLPXR dichroic mirror, and a 535DF25 emission filter. During the marked intervals, the cell was continuously illuminated through a 30% transmittance ND filter at 490 nm (490DF20; 0.40 W/cm^2) or 400 nm (400DF15; 0.14 W/cm^2) to induce photobleaching or photoactivation, respectively. (**F**) On/off cycles of Dronpa fluorescence observed using the same cell and filter set as in (E), except that excitation intensities were 1.3 W/cm^2 (490DF20) and 0.47 W/cm^2 (400DF15) for photobleaching and photoactivation, respectively. After 100 cycles, fluorescence intensity of the fully activated sample was 75% of the original level. (**G**) Six letters written successively on the same field of a cover slip overlaid with immobilized Dronpa protein. The time points of erasure at 488 nm and writing at 405 nm are indicated by arrowheads and arrows, respectively. Scale bar, 300 μm.

photobleaching, with respective quantum yields (Φ_{PA} and Φ_{PB}) of 0.37 and 0.00032. Fluorescence could be switched on and off repeatedly (Fig. 1F). The off state was thermally stable; <1% of the original intensity was recovered after incubation at 20°C for 10 min in the dark. Using a laser-scanning confocal microscope, we were also able to inscribe six letters on a cover slip with immobilized Dronpa protein (*8*) (Fig. 1G), showing that Dronpa is an information storage medium with the ability to record, erase, or read information nondestructively (*11*, *12*). Comparisons between Dronpa and photoactivatable (PA)-GFP (*5*) are shown in table S1. The relatively fast bleaching rate of Dronpa at 488 nm (Φ_{PB} = 0.00032) may be a drawback because a limited number of images can be acquired after photoactivation. However, because of the high Φ_{FL} (0.85), multiple bright images could be obtained when the excitation light was reasonably attenuated.

Although photochromism has been reported for the yellow-emitting variants (YFPs) of *Aequorea* GFP at the single-molecular level (*13*), they have not demonstrated appreciable photochromism when measured in bulk. After a single round of photobleaching with illumination at 490 nm, only a small fraction (10 to 40%) of the original intensity could be restored (*14*), and recovery did not necessarily require illumination with 400-nm light, indicating the thermal instability of the off state of YFP.

The perfect photochromic properties of Dronpa suggested that it would be a useful tool to analyze the heretofore unexplored regulation of fast protein dynamics. The mitogen-activated protein kinase [extracellular signal-regulated kinase (ERK)] signaling cascade transduces a variety of extracellular signals at multiple levels in the cell (*15*, *16*). Upon stimulation, ERK detaches from its cytosolic anchors and translocates into the nucleus, where it regulates gene expression by phosphorylating transcription factors. ERK is then returned to the cytoplasm through nuclear export mechanisms that are sensitive to leptomycin B, a specific inhibitor of nuclear export signal (NES)–mediated nuclear export. Previous studies with immunocytochemistry or GFP-fused ERK (*17*, *18*) have examined only nuclear accumulation upon leptomycin B treatment or the steady-state distribution of ERK between the nucleus and cytoplasm, which should be dictated by the relative strengths of the nuclear import and export flows.

To measure directly both nuclear influx and efflux of ERK, we tagged ERK1 with Dronpa (ERK1-Dronpa) and examined its behavior in COS7 cells upon stimulation with epidermal growth factor (EGF). Photobleaching and photoactivation of Dronpa and fluorescence measurements were performed with laser-scanning confocal microscopy. ERK1-Dronpa was initially distributed throughout the cytosol and nucleus (Fig. 2A). After fluorescence was erased to background levels with a strong 488-nm laser line (1.4 W/cm^2), Dronpa was photoactivated in part of the cytoplasm (Fig. 2B). As a result of the high quantum yield of the photoactivation process (Φ_{PA} = 0.37), the marking required only a single 200-ms scan using a 405-nm laser line (0.20 W/cm^2). Next, a series of images was acquired by using a weak 488-nm laser line (0.014 W/cm^2) (Fig. 2D). Within 40 s, a substantial gradient of fluorescence signal was apparent across the nuclear envelope, which suggests inefficient nuclear import of ERK1-Dronpa. After erasure, nuclear export was examined by tracing the fluorescence of ERK1-Dronpa photoactivated in a region inside the nucleus (Fig. 2B). Again, inefficient transport was observed (Fig. 2F).

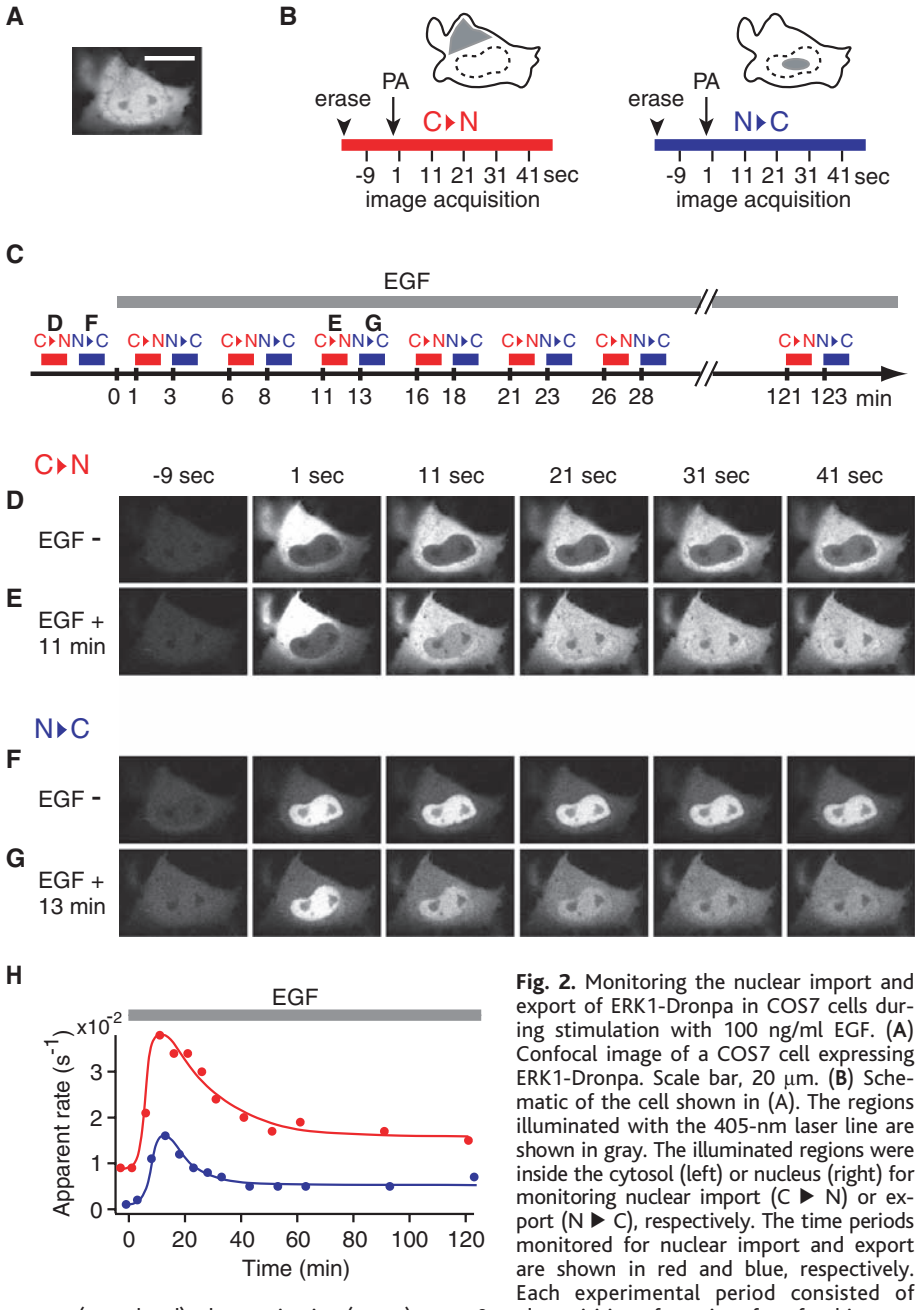

Fig. 2. Monitoring the nuclear import and export of ERK1-Dronpa in COS7 cells during stimulation with 100 ng/ml EGF. (**A**) Confocal image of a COS7 cell expressing ERK1-Dronpa. Scale bar, 20 μm. (**B**) Schematic of the cell shown in (A). The regions illuminated with the 405-nm laser line are shown in gray. The illuminated regions were inside the cytosol (left) or nucleus (right) for monitoring nuclear import (C ▶ N) or export (N ▶ C), respectively. The time periods monitored for nuclear import and export are shown in red and blue, respectively. Each experimental period consisted of erasure (arrowhead), photoactivation (arrow) at t = 0, and acquisition of a series of confocal images. (**C**) Timetable of intermittent monitoring of the nuclear import and export of ERK1-Dronpa before and during stimulation with EGF (gray bar). (**D** and **E**) Nuclear import of ERK1-Dronpa before stimulation (D) or after an 11-min incubation with EGF (E). (**F** and **G**) Nuclear export of ERK1-Dronpa before stimulation (F) or after a 13-min incubation with EGF (G). (**H**) Time courses of the nuclear influx (red) and efflux (blue) rates (*8*) of ERK1-Dronpa during EGF stimulation.

Next, these experiments were repeated eight times during continuous stimulation of the cell with 100 ng/ml EGF (Fig. 2C and movie S1). At early time points, the nucleocytoplasmic shuttling remained slow; however, 11 min after the onset of EGF stimulation, nuclear import was greatly enhanced (Fig. 2E). Interestingly, at a similar time point (13 min), nuclear export was also facilitated (Fig. 2G). This result contradicts a simple model in which a decrease in nuclear export accounts for nuclear accumulation of ERK. The rate of reduction of the fluorescence gradient across the nuclear envelope was quantified and plotted against time (Fig. 2H). The translocation of ERK1-Dronpa across the nuclear envelope was accelerated in both directions after several minutes of EGF stimulation. The phosphorylation of ERK1-Dronpa and its nuclear accumulation were confirmed by Western blotting and immunocytochemistry (fig. S3). The acceleration of the bidirectional flow of ERK1-Dronpa was also evident with lower concentrations of EGF (10 ng/ml), with the shuttling rate peaking with reduced amplitudes at similar or slightly later time points (fig. S4). Similar regulation was observed for ERK2-Dronpa in COS7 cells and HeLa cells that were stimulated with EGF. Thus, ERK signaling in the nucleus may be regulated by the rate of ERK nucleocytoplasmic shuttling. Assuming that ERK principally undergoes inactivation within the nucleus (*19*), fast circulation across the nuclear envelope is predicted to more effectively increase gene expression than does simple nuclear retention. Notably, variation in the initial shuttling rate between different cells was observed (fig. S5). Thus, any changes in movement must be assessed using data from a single cell, because measurements are affected by the geometry of the cells and marked regions.

Unlike ERK, nuclear localization signal (NLS)–containing proteins are transported by importins (*20*). The nuclear import of signal transduction and transcription factors, such as NF-κB and NF-AT, uses the NLS system. Importin β shuttles between the cytosol and nucleus as a translocation component by directly interacting with the nuclear pore complex (NPC). To observe the nucleocytoplasmic shuttling of importin β, we tagged importin β with Dronpa (importin-β-Dronpa). The chimeric protein was distributed throughout the cytosol and nucleus in COS7 cells, with some protein observed at the nuclear envelope (Fig. 3A). After erasure, Dronpa was photoactivated in a region of the cytosol (Fig. 3B) or nucleus (Fig. 3C) at $t = 0$, and a series of confocal images was acquired. Intense fluorescence at the nuclear envelope appeared immediately after photoactivation inside the cytosol or nucleus (Fig. 3, B and C), which suggests that both nuclear import and export of importin β involved direct interactions with the NPC. Because growth-factor stimulation changes the permeability of the nuclear envelope to NLS-containing gold particles (*21*), we quantified the shuttling rate of importin-β-Dronpa using the same protocol as for ERK1-Dronpa. The bidirectional flow rates were constant during incubation with 100 ng/ml EGF for 30 min (Fig. 3D), which suggests that the intrinsic nucleocytoplasmic shuttling of importin β was indifferent to growth-factor stimulation. The shuttling rate was variable between three different cells, stressing again the requirement for protein movement to be measured at multiple time points in individual cells.

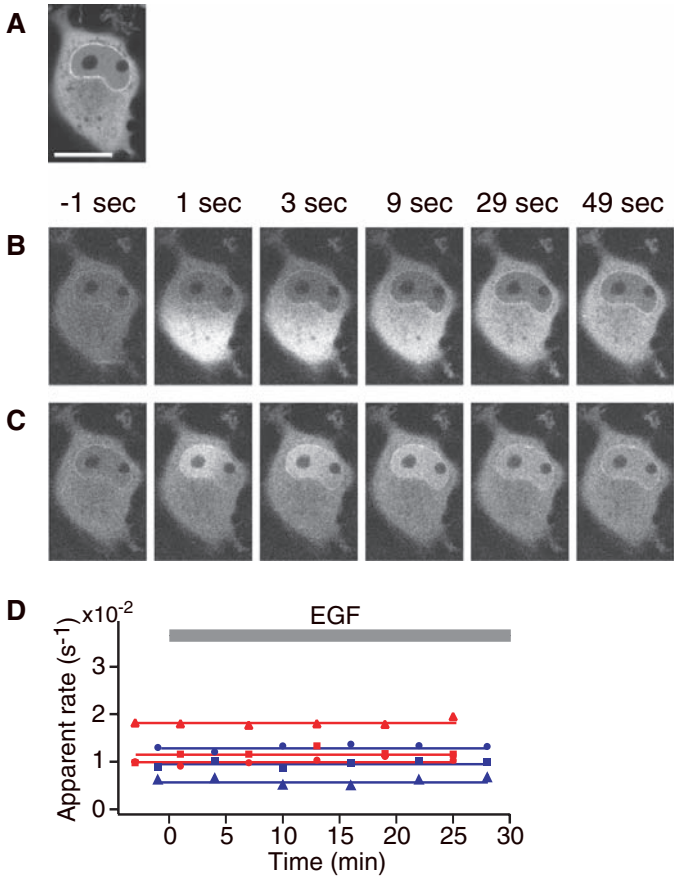

Fig. 3. Monitoring the nuclear import and export of importin-β-Dronpa in COS7 cells. (**A**) Confocal image of a COS7 cell expressing importin-β-Dronpa. Scale bar, 20 μm. (**B** and **C**) Nuclear import (B) and export (C) of importin-β-Dronpa. (**D**) Time courses of the nuclear influx (red) and efflux (blue) rates (*8*) of importin-β-Dronpa during stimulation with 100 ng/ml EGF, obtained from different three cells.

References and Notes

1. R. Y. Tsien, *Annu. Rev. Biochem.* **67**, 509 (1998).
2. J. Zhang, R. E. Campbell, A. Y. Ting, R. Y. Tsien, *Nature Rev. Mol. Cell Biol.* **3**, 906 (2002).
3. V. V. Verkhusha, K. A. Lukyanov, *Nature Biotechnol.* **22**, 289 (2004).
4. J. Lippincott-Schwartz, E. Snapp, A. Kenworthy, *Nature Rev. Mol. Cell Biol.* **2**, 444 (2001).
5. G. H. Patterson, J. Lippincott-Schwartz, *Science* **297**, 1873 (2002).
6. R. Ando, H. Hama, M. Yamamoto-Hino, H. Mizuno, A. Miyawaki, *Proc. Natl. Acad. Sci. U.S.A.* **99**, 12651 (2002).
7. D. M. Chudakov *et al.*, *Nature Biotechnol.* **21**, 191 (2003).
8. Materials and methods are available as supporting material on *Science* Online.
9. Y. A. Labas *et al.*, *Proc. Natl. Acad. Sci. U.S.A.* **99**, 4256 (2002).
10. R. E. Campbell *et al.*, *Proc. Natl. Acad. Sci. U.S.A.* **99**, 7877 (2002).
11. M. Irie, T. Fukaminato, T. Sasaki, N. Tamai, T. Kawai, *Nature* **420**, 759 (2002).
12. Y. C. Liang, A. S. Dvornikov, P. M. Rentzepis, *Proc. Natl. Acad. Sci. U.S.A.* **100**, 8109 (2003).
13. R. M. Dickson, A. B. Cubitt, R. Y. Tsien, W. E. Moerner, *Nature* **388**, 355 (1997).
14. A. Miyawaki, R. Y. Tsien, *Methods Enzymol.* **327**, 472 (2000).
15. T. S. Lewis, P. S. Shapiro, N. G. Ahn, *Adv. Cancer Res.* **74**, 49 (1998).
16. M. J. Robinson, M. H. Cobb, *Curr. Opin. Cell Biol.* **9**, 180 (1997).
17. T. Furuno, N. Hirashima, S. Onizawa, N. Sagiya, M. Nakanishi, *J. Immunol.* **166**, 4416 (2001).
18. A. M. Horgan, P. J. S. Stork, *Exp. Cell Res.* **285**, 208 (2003).
19. V. Volmat, M. Camps, S. Arkinstall, J. Puoyssegur, P. Lenormand, *J. Cell Sci.* **114**, 3433 (2001).
20. L. Xu, J. Massagué, *Nature Rev. Mol. Cell Biol.* **5**, 209 (2004).
21. C. M. Feldherr, D. Akin, *Exp. Cell Res.* **205**, 179 (1993).

22. We thank S. Karasawa for preparation of coral and for valuable advice, M. Cobb for the ERK1 construct, Y. Yoneda for the human importin β1 construct, and S. Habuchi, J. Hofkens, Y. Gotoh, N. Imamoto, Y. Sato, K. Takishima, and C. Bargmann for critical comments. This work was partly supported by grants from the Japanese Ministry of Education, Science, and Technology, from the Human Frontier Science Program, and from the New Energy and Industrial Technological Development Organization.

Supporting Online Material

www.sciencemag.org/cgi/content/full/306/5700/1370/DC1
Materials and Methods
Figs. S1 to S5
Table S1
Movie S1

8 July 2004; accepted 3 September 2004